

LA-UR-12-00155

Approved for public release;
distribution is unlimited.

Title: Continuous-S(α , β) Capability in MCNP

Author(s): Jeremy Lloyd Conlin
D. Kent Parsons
Forrest B. Brown
Robert E. MacFarlane
Robert C. Little
Morgan C. White

Intended for: 2012 ANS Annual Meeting
Chicago, IL
June 24–28, 2012



Los Alamos National Laboratory, an affirmative action/equal opportunity employer, is operated by the Los Alamos National Security, LLC for the National Nuclear Security Administration of the U.S. Department of Energy under contract DE-AC52-06NA25396. By acceptance of this article, the publisher recognizes that the U.S. Government retains a nonexclusive, royalty-free license to publish or reproduce the published form of this contribution, or to allow others to do so, for U.S. Government purposes. Los Alamos National Laboratory requests that the publisher identify this article as work performed under the auspices of the U.S. Department of Energy. Los Alamos National Laboratory strongly supports academic freedom and a researcher's right to publish; as an institution, however, the Laboratory does not endorse the viewpoint of a publication or guarantee its technical correctness.

Continuous- $S(\alpha, \beta)$ Capability in MCNP

Jeremy Lloyd Conlin, D. Kent Parsons, Forrest B. Brown, Robert E. MacFarlane, Robert C. Little, and Morgan C. White

Los Alamos National Laboratory
PO Box 1663, Los Alamos NM 87544

INTRODUCTION

For many years MCNP [1] has had the ability to handle $S(\alpha, \beta)$ thermal scattering [2]. MCNP uses ENDF [3] data processed through NJOY [4] to produce $S(\alpha, \beta)$ data tables. Traditionally, these data tables have used a discrete representation of the secondary neutron spectrum and angular distribution following a scattering reaction at thermal (i.e., < 4 eV) energies. From this discrete representation, the secondary neutron was limited to a discrete energy and discrete angle while the scattering physics theory provides no such limitation. The use of the discrete representation does not produce noticeable effects in integral calculations such as eigenvalue (i.e., k -effective) calculations [5], but can produce noticeable deficiencies for differential calculations [6].

The discrete $S(\alpha, \beta)$ representation output by NJOY and used by MCNP was originally designed to conserve space for the limited storage capabilities of computers in the early 1980s [7]. In the early 1990s it was discovered that this discrete representation produced some unphysical anomalies [8].

A new representation of the $S(\alpha, \beta)$ data was created in 2006 and implemented in MCNP in 2008 [9]. $S(\alpha, \beta)$ data files have been available online since 2007 [8]—although their availability has not been widely known. This summary reports on this new format, the processing of the ENDF/B-VII.0 data, and some sample calculations illustrating the impact of the new format.

NEW CONTINUOUS-ENERGY $S(\alpha, \beta)$ FORMAT

The new $S(\alpha, \beta)$ representation provides a continuous-energy and angle distribution for secondary neutrons from a scattering reaction at thermal energies. This new continuous-energy format does not require a new ENDF evaluation and is processed through NJOY slightly differently than for the discrete representation. To obtain the discrete (traditional) representation, the *iwt* variable—seventh entry on card 9 of the ACER—input is set to 0; for the continuous-energy representation, *iwt* is set to 2.

The formats for the discrete and continuous-energy representations will not be detailed here. The documentation for the discrete $S(\alpha, \beta)$ representation format can be found in Appendix F, Volume III of the MCNP5 manual. As of January 2012, this document is currently being revised—including adding documentation for the continuous- $S(\alpha, \beta)$ representation format—and will be made publicly available upon its completion. A more detailed discussion of the processing and

testing of the continuous representation of the $S(\alpha, \beta)$ data can be found in the memo by Conlin et al. [10].

SAMPLE CALCULATIONS

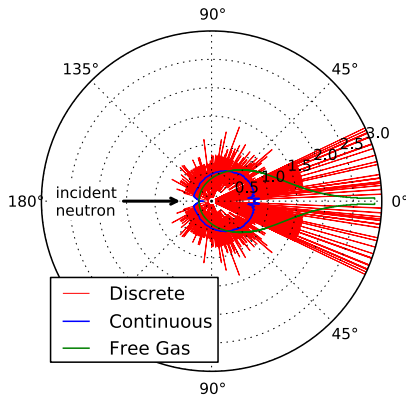
Cullen et al. [6] demonstrated in 2003 problems that may arise when performing differential calculations using a discrete representation of the $S(\alpha, \beta)$ data. The calculation performed was a “broomstick” problem which consists of a very thin (10^{-8} cm radius) and very long (10^5 cm) cylinder with a monoenergetic (0.0253 eV) point source located on the axis of the cylinder 10^3 cm from one end and directed along the axis of the cylinder. Outside the “broomstick” is a vacuum and neutrons are tallied on infinite planes perpendicular to the cylinder; the tallies were binned in energy and in angle representing the secondary neutron spectrum and angular distribution. With a virtually infinitesimally thin and infinitely long cylinder, any neutron that scatters within the cylinder will escape the cylinder and travel in a straight line to the planes where it is tallied.

Cullen et al. observed that the discrete representation of the $S(\alpha, \beta)$ data as used in MCNP gives “spikes” in the secondary neutron spectrum and angular distribution tallies; these spikes are akin to the ray effects seen in discrete ordinates calculations [11] and are unphysical.

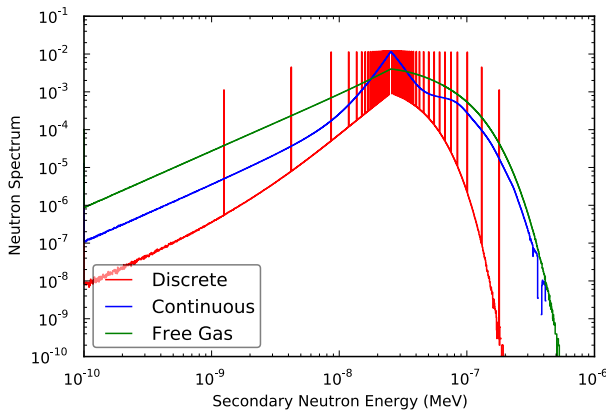
To illustrate the effects of using the different $S(\alpha, \beta)$ representations, we have run a slightly modified version of the broomstick problem; the only change from the broom stick problem by Cullen et al. is the location of our point source is just inside (10^{-12} cm) one end of the cylinder instead of 10^3 cm from one end. Like Cullen et al., we tallied the current over infinite planes perpendicular to the ends of cylinder. The tallies were binned in either energy or in cosine. The energy bins were 2000 logarithmically spaced bins from 10^{-10} MeV to 10^{-5} MeV. The cosine bins were slightly more complicated as we were trying to capture the angular distribution for very forward peaked scatters. The cosine tally was binned into 500 bins from -1.0 to 0.9 , 250 bins from 0.9 to 0.99 and 100 bins from 0.99 to 1.0 . We performed our calculation for both the discrete and continuous representations of the $S(\alpha, \beta)$ thermal scattering treatment as well as without the $S(\alpha, \beta)$ thermal scattering treatment for comparison. In all of our calculations the $S(\alpha, \beta)$ evaluation is hydrogen in light water; $S(\alpha, \beta)$ scattering off of oxygen is not represented here.

The results of these calculations are shown in Figures 1; Figure 1(a) shows the secondary-angular distribution on a polar plot and Figure 1(b) shows the secondary-neutron spectrum. The red and blue lines show the tally results for the

discrete- and continuous- $S(\alpha, \beta)$ representations respectively; the green lines show the tally results when the $S(\alpha, \beta)$ thermal scattering treatment is not used (i.e., no mt card in MCNP). Note that the angular distribution for the discrete representation was cut off for any bin values above 3; those bin values were all approximately 5.73. The uncertainty in the values are all less than 1%. Further note that the MCNP tallies were binned in angle from -1 to 1 in cosine space which corresponds to 0° to 180° in Figure 1(a). The top and bottom of Figure 1(a) contain the same data and are plotted in polar format to illustrate the secondary-angle distribution.



(a) Angle



(b) Energy

Fig. 1: Secondary neutron distribution following scattering reaction off of H_2O molecule. Note that the angular distribution for the discrete case is cut off; the values for the 0° to 30° are approximately 5.73.

In Figure 1(a) we see the same effects in the angular distribution using the discrete $S(\alpha, \beta)$ representation that Cullen et al. lamented in their paper, namely, the unphysical spikes. The new continuous representation shows a smoothly varying angular distribution that is slightly forward peaked. For comparison, the secondary angle distribution for the free gas model (i.e., no $S(\alpha, \beta)$ treatment) shows a very forward peaked distri-

bution.

In Figure 1(b) is shown the secondary neutron spectrum. When using the discrete $S(\alpha, \beta)$ representation, we see a background spectrum with superimposed spikes. The background comes from scattering off of the oxygen nuclei and is qualitatively the same as the free gas model (no $S(\alpha, \beta)$ scattering treatment) shown in green. The spikes are from scattering off of hydrogen nuclei to specific or discrete secondary energies. The continuous results show a more integrated, or smeared out, result as expected.

CONCLUSION

Using the existing/discrete representation of $S(\alpha, \beta)$ data in MCNP the results that Cullen et al. have shown in their paper [6] for the so-called broomstick problem have been replicated. New $S(\alpha, \beta)$ data tables using the continuous- $S(\alpha, \beta)$ representation have been created and used on the same broomstick problem.

The comparison of the tally results from the discrete- and continuous- $S(\alpha, \beta)$ representation show an improvement of the representation of the physics using the continuous- $S(\alpha, \beta)$ representation. It is our opinion that the continuous representation should always be used.

We have only shown in this paper the results from a calculation with water as the medium through which neutrons are transported. Water was chosen as it is a common material and it is representative of other results we have seen in similar calculations with other materials. Space constrains us from including those results in this paper.

AVAILABILITY OF CONTINUOUS-ENERGY $S(\alpha, \beta)$ FILES

The continuous- $S(\alpha, \beta)$ representation data tables will be distributed with MCNP6 when it is released. All of the $S(\alpha, \beta)$ data tables referenced in this paper come from the ENDF/B-VII.0 evaluation. Once the ENDF/B-VII.1 evaluation is released and processed with NJOY, the $S(\alpha, \beta)$ data tables will be made available in both the discrete and continuous representations.

A list of ZAIDs for discrete- and continuous- $S(\alpha, \beta)$ representations (from the ENDF/B-VII.0 evaluation) and their associated temperatures are listed in Table I. The ZAIDs for discrete $S(\alpha, \beta)$ representations have been already been distributed in MCNP since 2008 [12].

A list of the $S(\alpha, \beta)$ ZAID prefixes and the material referenced by that prefix is included here.

al27	Aluminium-27
be	Beryllium Metal
be/o	Beryllium in Beryllium Oxide
benz	Benzene
dortho	Ortho Deuterium
dpara	Para Deuterium

fe56	Iron-56
grph	Graphite
h/zr	Hydrogen in Zirconium Hydride
hortho	Ortho Hydrogen
hpara	Para Hydrogen
hwtr	Deuterium in Heavy Water
lmeth	Hydrogen in Liquid Methane
lwtr	Hydrogen in Light Water
o/be	Oxygen in Beryllium Oxide
o2/u	Oxygen in UO ₂
poly	Hydrogen in Polyethylene
smeth	Hydrogen in Solid Methane
u/o2	Uranium-238 in UO ₂
zr/h	Zirconium in Zirconium Hydride

REFERENCES

1. X-5 Monte Carlo Team, MCNP—A General N-Particle Transport Code, Version 5, in *Trans. Am. Nucl. Soc.*, American Nuclear Society (November 2002), vol. 87, p. 273.
2. F. G. Bischoff, M. L. Yeater, and W. E. Moore, Monte Carlo Evaluation of Multiple Scattering and Resolution Effects in Double-Differential Neutron Scattering Cross-Section Measurements, *Nuclear Science and Engineering*, **48**, 3, pp. 266–& (1972).
3. M. B. Chadwick, P. Obložinský, M. Herman, N. M. Greene, R. D. McKnight, D. L. Smith, P. G. Young, R. E. MacFarlane, G. M. Hale, S. C. Frankle, A. C. Kahler, T. Kawano, R. C. Little, D. G. Madland, P. Moller, R. D. Mosteller, P. R. Page, P. Talou, H. Trellue, M. C. White, W. B. Wilson, R. Arcilla, C. L. Dunford, S. F. Mughabghab, B. Pritychenko, D. Rochman, A. A. Sonzogni, C. R. Lubitz, T. H. Trumbull, J. P. Weinman, D. A. Brown, D. E. Cullen, D. P. Heinrichs, D. P. McNabb, H. Derrien, M. E. Dunn, N. M. Larson, L. C. Leal, A. D. Carlson, R. C. Block, J. B. Briggs, E. T. Cheng, H. C. Huria, M. L. Zerkle, K. S. Kozier, A. Courcelle, V. Pronyaev, and S. C. van der Marck, ENDF/B-VII.0: Next generation evaluated nuclear data library for nuclear science and technology, *Nuclear Data Sheets*, **107**, 12, pp. 2931–3059 (Dec. 2006).
4. R. E. MacFarlane and A. C. Kahler, Methods for Processing ENDF/B-VII with NJOY, *Nuclear Data Sheets*, **111**, 12, pp. 2739–2889 (Dec. 2010).
5. A. T. Pavlou, F. B. Brown, W. R. Martin, and B. C. Kiedrowski, Comparison of Discrete and Continuous Thermal Neutron Scattering Treatments in MCNP5, in *PHYSOR 2012—Advances in Reactor Physics—Linking Research, Industry, and Education*, American Nuclear Society, LaGrange Park, IL (April 15–20 2012).
6. D. E. Cullen, L. F. Hansen, E. M. Lent, and E. F. Plechaty, Thermal Scattering Law Data: Implementation and Testing using the Monte Carlo neutron transport codes COG, MCNP and TART, Tech. Rep. UCRL-ID-153656, Lawrence Livermore National Laboratory (May 17 2003).
7. R. E. MacFarlane, A discussion of the MCNP Thermal Scattering Model, (March 22 2005).
8. R. E. MacFarlane, personal communication (January 2012).
9. T. E. Booth, F. B. Brown, J. S. Bull, R. A. Forster, J. T. Goorley, H. G. Hughes, R. L. Martz, R. E. Prael, A. Sood, J. E. Sweezy, and A. J. Zukaitis, MCNP5 1.50 Release Notes, Tech. Rep. LS-UR-08-2300, Los Alamos National Laboratory (2008).
10. J. L. Conlin and D. K. Parsons, Release of Continuous Representation for $S(\alpha, \beta)$ ACE Data, Tech. Rep. XCP-5:12-012, Los Alamos National Laboratory (2012).
11. K. D. Lathrop, Ray Effects in Discrete Ordinates Equations, *Nuclear Science and Engineering*, **32**, 3, pp. 357–& (1968).
12. H. R. Trellue and R. C. Little, Release of New MCNP S(alpha,beta) Library ENDF70SAB Based on ENDF/B-VII.0, Tech. Rep. LA-UR-08-3628, Los Alamos National Laboratory (2008).

TABLE I: Discrete and continuous ZAIDs and temperatures for $S(\alpha, \beta)$ libraries.

Discrete ZAID	Continuous ZAID	Temp. (K)	Discrete ZAID	Continuous ZAID	Temp. (K)	Discrete ZAID	Continuous ZAID	Temp. (K)
al27.10t	al27.20t	20	grph.10t	grph.20t	293.6	o/be.10t	o/be.20t	293.6
al27.11t	al27.21t	80	grph.11t	grph.21t	400	o/be.11t	o/be.21t	400
al27.12t	al27.22t	293.6	grph.12t	grph.22t	500	o/be.12t	o/be.22t	500
al27.13t	al27.23t	400	grph.13t	grph.23t	600	o/be.13t	o/be.23t	600
al27.14t	al27.24t	600	grph.14t	grph.24t	700	o/be.14t	o/be.24t	700
al27.15t	al27.25t	800	grph.15t	grph.25t	800	o/be.15t	o/be.25t	800
be.10t	be.20t	293.6	grph.16t	grph.26t	1000	o/be.16t	o/be.26t	1000
be.11t	be.21t	400	grph.17t	grph.27t	1200	o/be.17t	o/be.27t	1200
be.12t	be.22t	500	grph.18t	grph.28t	1600	o2/u.10t	o2/u.20t	293.6
be.13t	be.23t	600	grph.19t	grph.29t	2000	o2/u.11t	o2/u.21t	400
be.14t	be.24t	700	h/zr.10t	h/zr.20t	293.6	o2/u.12t	o2/u.22t	500
be.15t	be.25t	800	h/zr.11t	h/zr.21t	400	o2/u.13t	o2/u.23t	600
be.16t	be.26t	1000	h/zr.12t	h/zr.22t	500	o2/u.14t	o2/u.24t	700
be.17t	be.27t	1200	h/zr.13t	h/zr.23t	600	o2/u.15t	o2/u.25t	800
be/o.10t	be/o.20t	293.6	h/zr.14t	h/zr.24t	700	o2/u.16t	o2/u.26t	1000
be/o.11t	be/o.21t	400	h/zr.15t	h/zr.25t	800	o2/u.17t	o2/u.27t	1200
be/o.12t	be/o.22t	500	h/zr.16t	h/zr.26t	1000	poly.10t	poly.20t	293.6
be/o.13t	be/o.23t	600	h/zr.17t	h/zr.27t	1200	poly.11t	poly.21t	350
be/o.14t	be/o.24t	700	hortho.10t	hortho.20t	20	smeth.10t	smeth.20t	22
be/o.15t	be/o.25t	800	hpara.10t	hpara.20t	20	u/o2.10t	u/o2.20t	293.6
be/o.16t	be/o.26t	1000	hwtr.10t	hwtr.20t	293.6	u/o2.11t	u/o2.21t	400
be/o.17t	be/o.27t	1200	hwtr.11t	hwtr.21t	350	u/o2.12t	u/o2.22t	500
benz.10t	benz.20t	293.6	hwtr.12t	hwtr.22t	400	u/o2.13t	u/o2.23t	600
benz.11t	benz.21t	350	hwtr.13t	hwtr.23t	450	u/o2.14t	u/o2.24t	700
benz.12t	benz.22t	400	hwtr.14t	hwtr.24t	500	u/o2.15t	u/o2.25t	800
benz.13t	benz.23t	450	hwtr.15t	hwtr.25t	550	u/o2.16t	u/o2.26t	1000
benz.14t	benz.24t	500	hwtr.16t	hwtr.26t	600	u/o2.17t	u/o2.27t	1200
benz.15t	benz.25t	600	hwtr.17t	hwtr.27t	650	zr/h.10t	zr/h.20t	293.6
benz.16t	benz.26t	800	lmeth.10t	lmeth.20t	100	zr/h.11t	zr/h.21t	400
benz.17t	benz.27t	1000	lwtr.10t	lwtr.20t	293.6	zr/h.12t	zr/h.22t	500
dortho.10t	dortho.20t	19	lwtr.11t	lwtr.21t	350	zr/h.13t	zr/h.23t	600
dpara.10t	dpara.20t	19	lwtr.12t	lwtr.22t	400	zr/h.14t	zr/h.24t	700
fe56.10t	fe56.20t	20	lwtr.13t	lwtr.23t	450	zr/h.15t	zr/h.25t	800
fe56.11t	fe56.21t	80	lwtr.14t	lwtr.24t	500	zr/h.16t	zr/h.26t	1000
fe56.12t	fe56.22t	293.6	lwtr.15t	lwtr.25t	550	zr/h.17t	zr/h.27t	1200
fe56.13t	fe56.23t	400	lwtr.16t	lwtr.26t	600			
fe56.14t	fe56.24t	600	lwtr.17t	lwtr.27t	650			
fe56.15t	fe56.25t	800	lwtr.18t	lwtr.28t	800			